Brazilian Journal
of Chemical
Engineering

ISSN 0104-6632
Printed in Brazil
www.abeq.org.br/bjche

Vol. 29, No. 01, pp. 167 - 182, January - March, 2012

TIME-FREQUENCY ANALYSIS OF HILBERT SPECTRUM OF PRESSURE FLUCTUATION TIME SERIES IN A KENICS STATIC MIXER BASED ON EMPIRICAL MODE DECOMPOSITION

Huibo Meng, Zhiqiang Liu, Yanfang Yu* and Jianhua Wu

Key Laboratory of Liaoning Province for Efficient Chemical Mixing Technology,
College of Mechanical Engineering, Phone: + 86-24-89385408, Fax + 86-24-89381016,
Shenyang University of Chemical Technology, Shenyang 110142, P.R. China.
E-mail: mhb_vip@163.com

(Submitted: January 15, 2011 ; Revised: October 6, 2011 ; Accepted: October 10, 2011)

Abstract - The turbulent flow in a Kenics Static Mixer (KSM) was intensified under the mutual-coupling effect between the twisted leaves and the tube-wall. In order to understand the intrinsic features of turbulent flow in KSM, the Hilbert-Huang Transform based on Empirical Mode Decomposition were first introduced to describe the time-frequency features of the pressure fluctuation. The Hilbert spectra of pressure fluctuation time series were quantitatively evaluated under different Reynolds numbers, and different radial and axial positions, respectively. The experimental results showed that: the fluctuation frequencies of pressure signals in a KSM were mainly distributed below 40 Hz, and more than 68% of the energy of signals is concentrated within 10 Hz. Compared with the other IMFs, the pressure component of C_6 in the range of 7.82~15.63 Hz has the maximum fluctuation energy ratio. As the flow rate increases, the energy of fluctuation of fluid micelles and the proportion of low-frequency energy increases. The pressure fluctuation with higher energy ratio of low frequency (0~10 Hz) had lower amplitudes at r/R=0.3 because of the core of forced vortex. Nevertheless, the effect of the free vortex was that the pressure fluctuation with lower energy ratio of low frequency had higher amplitudes at r/R=0.8. The higher amplitudes of pressure fluctuation at cross sections of CS3 (z=420 mm) and CS5 (z=620 mm) proved that the transitions between the adjacent mixing element had better mixing performance.
Keywords: Static mixer; Pressure fluctuation; Hilbert-Huang transform; Empirical mode decomposition.

INTRODUCTION

Static mixers, also known as motionless mixers, have become standard intensification equipment in the chemical process industries. During the past several decades, static mixers have been widely used in chemical industries for a variety of mixing processes such as gas-liquid, liquid-liquid, and gas-liquid-solid systems (Thakur *et al*., 2003). Compared with conventional mixing devices, static mixers can achieve better performance at lower cost, smaller space requirement, shorter residence time and lower energy consumption (Lisboa *et al*., 2010; Madhuranthakam *et al*., 2009). As far as the potential advantages of static mixers are concerned, new designs are being developed and new applications are being explored (Krstic *et al*., 2007; Lisboa *et al*., 2010; Madhuranthakam *et al*., 2009).

Static mixers consist of mixing elements placed on the inside of a pipe. The elements are fixed and do not move. Chemicals, which are added just upstream of the elements, mix with the bulk fluid because of the complex, three-dimensional fluid motion that is generated by the elements (Jones *et*

*To whom correspondence should be addressed

al., 2002). The purpose of the elements is to redistribute fluid in the directions transverse to the main flow, i.e., in the radial and tangential directions. As a result, the shape of the elements determines the character of this fluid motion and thus determines the effectiveness of the mixer. One typical static mixer, the Kenics static mixer (the so-called standard mixer) has been on the market for about 60 years. In previous studies on static mixers, characteristics such as residence time distributions, pressure drop, stretching rates, and degree of mixing have been investigated experimentally (Chen, 1973; Grace, 1971; Pahl and Muschelknautz, 1982; Wilkinson and Cliff, 1977; Wu *et al*., 2008, 2009, 2010; Zhang *et al*., 2006), as well as numerically, using computational fluid dynamics (Byrde and Sawley, 1999; Hobbs and Muzzio, 1997, 1998a, 1998b; Hobbs *et al*., 1998; Joshi *et al*., 1995; Kumar *et al*., 2008; Mårten *et al*., 2006, 2008; Rauline *et al*., 1998; Visser *et al*., 1999; Zalc *et al*., 2002). Yet, they have not been well characterized due to the complexity of the flow structure inside static mixers (Mårten *et al*., 2006, 2008)

Except for high viscosity liquids, the flow conditions of fluid mixing in most static mixers were considered to be as turbulent flow, which contains a series of eddies with a wide range of time and length scales and hence helps to promote macro- and micro mixing. Therefore, the spiral turbulence in the Kenics static mixer is a nonlinear chaotic dynamical system (Hobbs and Muzzio, 1997). The unsteady characteristics of turbulent flow in KSM are of interest and have received more attention during the past years. In order to evaluate the effect of number of mixing elements on the velocity distribution and turbulence, the flow field inside a KSM 0.04 m in diameter and 1.25 in aspect ratio was measured using a Laser Doppler Velocimeter (Wu *et al*., 2008). The self-correlation and mutual-correlation functions were utilized to study the linear and nonlinear correlation of the velocity fluctuation signal in the KSM over various frequency bands (Yu *et al*., 2008). Meng *et al*., (2009a) used the correlation dimension and Kolmogorov entropy to study the chaotic flow field of a KSM. The power spectrum and Maximum Lyapunov Exponent were used to distinguish the chaotic characteristic of the velocity signal in a KSM (Meng *et al*., 2009b). However, the sampled time series measured with the Laser Doppler Velocimeter had non-uniform time intervals which depend on the frequency and number of tracer particles flowing past the monitored points.

Therefore, it is necessary to have reliable methods for an experimental mapping of the complex and unsteady flow. On the other hand, pressure measurements are simple, reliable and possible to carry out under industrial conditions. Knowledge of pressure fluctuation characteristics in a KSM is important for chemical engineers for increasing the temperature of a reaction mixture or the removal of heat of reaction in a static mixer. The most widely used method to analyze pressure fluctuations uses linear tools, time domain (standard deviation) and the frequency domain (power spectral density function); however, as the static mixing dynamics can be interpreted as deterministic chaos, non-linear tools have also been used. The non-linear analysis of a time series of pressure fluctuations has been demonstrated to be an excellent tool for characterizing static mixing dynamics. The appropriate space dimension and delay for Lyapunov exponents must be known, but the delay value determined as described in literature is uncertain and affects the quality of the reconstructed attractor. A detailed review of the other non-stationary data processing methods (e.g., Fourier analysis, wavelet analysis, Wigner-Ville distribution, etc) has been made by Huang *et al*. (1998). A very appealing feature of the wavelet analysis is that it provides a uniform resolution for all the scales. Limited by the size of the basic wavelet function, the downside of the uniform resolution is uniformly poor resolution. Unlike the wavelet analysis, the instantaneous frequency from HHT can still be localized in time even for the longest period component without spreading energy over wide frequency and time ranges. Until recently, not enough reports on the instantaneous pulsating pressure signals except for tube-wall pressure (Wu *et al*. 2009) were found in the literatures for the chaotic flow systems. This gap in the literature motivated the authors of this report to undertake the task of analysis of frequency distribution based on Hilbert-Huang Transform and Empirical Mode Decomposition, which were first introduced to evaluate the time series in static mixers. The HHT method provided a new analytical tool for the complex flow structure in a static mixer. In this paper, the local time-frequency characteristics and energy characteristics were extracted from the pressure fluctuation signals under different Reynolds number, and radial and axial positions, respectively.

HILBERT-HUANG TRANSFORM FUNDAMENTAL PRINCIPLES

The Hilbert-Huang transform (HHT) proposed by Huang (1998) has adaptive characteristics without selecting a basic function. HHT mainly includes two

aspects: First, the primary signals are decomposed into a series of time-dependent intrinsic mode functions (IMFs). Second, instantaneous frequency and amplitude are obtained and presented in the three dimensional spectrum for every IMF, named as the Hilbert-Huang spectrum.

Empirical Mode Decomposition

Nonlinear and non-stationary complex signals can be decomposed into a number of intrinsic mode functions (IMFs). This process is known as empirical mode decomposition (EMD). The IMF must be satisfied with the following two conditions:

(a) In the whole data set, the number of extrema and the number of zero crossings must be equal or different at most by one.

(b) At any point, the mean value of the envelope defined by the local maxima and the envelope defined by the local minima is zero.

Sifting processes of Intrinsic Mode Functions are described as follows:

(a) Find all the extreme points of the time series s(t).

(b) Connect all the extreme points by cubic spline curves to structure upper and lower envelopes.

(c) Compute the average of the upper and lower envelopes $p_m(t)$.

(d) Calculate the difference between the signal s(t) and $p_m(t)$, named k(t), i.e.

$$k(t) = s(t) - p_m(t) \tag{1}$$

(e) Treat k(t) as an original signal, and repeat the steps (a) - (d), until k(t) satisfies the definition of an IMF, designated as $C_1(t)$.

(f) Separate $C_1(t)$ from the signal s(t), i.e.

$$rr_1(t) = s(t) - C_1(t) \tag{2}$$

(g) Treat $rr_1(t)$ as s(t), repeat the aforementioned process to obtain $C_1(t)$, $C_2(t)$, $C_3(t)$, ……, $C_m(t)$ until $rr_m(t)$ is a monotone function or a direct current component.

After EMD, the signal s(t) is decomposed into a series of IMF components $C_1(t)$, $C_2(t)$, $C_3(t)$, ……, $C_m(t)$ and a residual $rr_m(t)$. In other words,

$$s(t) = \sum_{j=1}^{m} C_j(t) + rr_m(t) \tag{3}$$

With the EMD method, each IMF component will satisfy the conditions of a Hilbert transform.

Hilbert Transform and Hilbert Spectrum

For each IMF component, its Hilbert transform is defined as

$$H_j(t) = \frac{1}{\pi} P \int \frac{C_j(\tau)}{t-\tau} d\tau \tag{4}$$

where P is the Cauchy principal value. With the Hilbert transform, the analytical signal is defined as

$$Z_j(t) = C_j(t) + iH_j(t) = a_j(t)e^{i\theta(t)} \tag{5}$$

in which the amplitude function $a_j(t)$ and phase function $\theta_j(t)$ can be described as following:

$$\begin{cases} a_j(t) = \sqrt{C_j(t)^2 + H_j(t)^2} \\ \theta_j(t) = \arctan[H_j(t) / C_j(t)] \end{cases} \tag{6}$$

So, the instantaneous frequency can be expressed as:

$$\omega_j(t) = d\theta_j(t) / dt \tag{7}$$

The amplitude function and instantaneous frequency function are both functions of time. For this reason, the amplitude can be presented on time-frequency plane, and the Hilbert-Huang spectrum is obtained:

$$H(\omega, t) = \text{Real}\left[\sum_{j=1}^{n} a_j(t) e^{i\int \omega_j(t)dt}\right] \tag{8}$$

where Real[] is the function for the real part of complex numbers. With the Hilbert-Huang spectrum defined, the marginal spectrum, h(ω), can be defined as:

$$h(\omega) = \int_0^T H(\omega, t)dt \tag{9}$$

where h(ω) means the magnitude of total amplitude of instantaneous frequency in the signals. And the marginal energy spectrum is defined as:

$$ES(\omega) = \int_0^T H^2(\omega, t)dt \tag{10}$$

where ES(ω) expresses the energy accumulation of each frequency within the time length.

EXPERIMENT

Experimental Equipment

The experimental apparatus, shown in Figure 1, consists mainly of the static mixing system and the high-speed data acquisition system. The KSM-unit, made of stainless steel, consisted of 6 helical elements placed at an angle of 90° to each other. Each element, 0.1 m in diameter and 0.2 m in length, twists left or right through an angle of 180°. Six pressure transducers (CGY4100, Chengdu Test Research Centre of Transducer, P. R. China) were installed on the walls of the mixer at the levels of CS1, CS2, CS3, CS4, CS5, CS6 to measure gauge pressure fluctuations, respectively. Detailed information on the measurement points is described in Figure 2. Each pressure probe was connected to one of the two input channels of a gauge pressure transducer, which produced an output voltage proportional to the pressure difference between the two channels. The remaining channel was exposed to the atmosphere. The differential range of the pressure transducer was 0~10 KPa, and the relative accuracy was ±0.01% full scale.

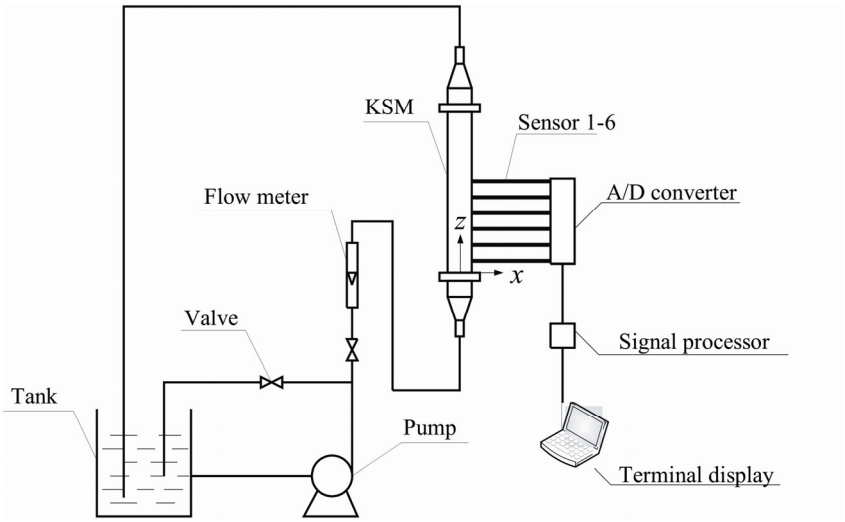

Figure 1: Schematic diagram of the experimental set-up for the pressure signal

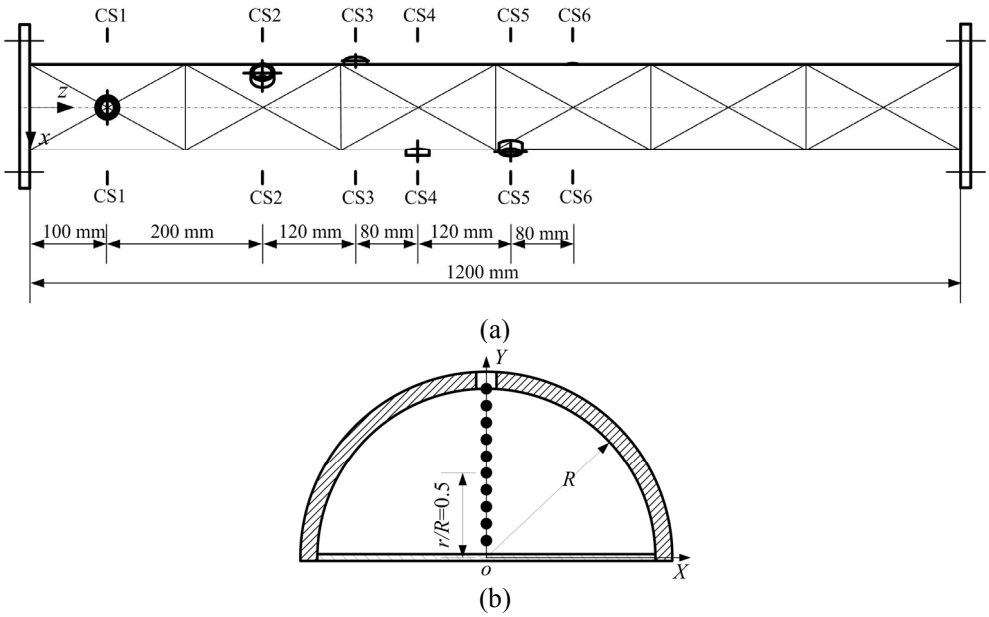

Figure 2: The arrangements of (a) axial and (b) radial direction measurement points for pressure conductors

Measurement Conditions

The medium employed in the circulating system was deionized water (ρ=998 kg.m^{-3}, μ=1.005×10^{-3} Pa·s). The experimental superficial inlet volume flow ranged from 500 to 1000 L·h^{-1} (i.e., Re=1756~3512), which is considered to be in the turbulent flow regimes in KSM (Chen *et al*., 2004). Considering that the locations of the axial cross-section of the mixing elements are diversified but have a periodic rule, a standard semicircular plane is described. The coordinate system of the standard plane is denoted by X and Y, which were span-wise or wall-normal for the cross-section of mixing elements. So the coordinate x and y of particles in different cross-sections can be transformed to coordinate X and Y with the equations following:

$$\begin{cases} X = \cos\alpha \cdot x + \sin\alpha \cdot y \\ Y = -\sin\alpha \cdot x + \cos\alpha \cdot y \end{cases} \tag{11}$$

and

$$\alpha = (-1)^{n-1} \frac{z-(n-1)l}{l} \cdot \pi + \left(\frac{\pi}{2}\right)^{n-1} \tag{12}$$

where α, l and n stand for the angle between the axial cross-section and the positive axis, the length of the mixing-element and the number of the mixing element at which the point i located, respectively.

At the standard semicircular plane, 10 measured points were evenly arranged on the radial axis as illustrated in Figure 2b. The time series consisted of at least 80000 points and were sampled at a frequency of 500 Hz using an analog-to-digital converter with 12 bit nominal resolution. A low-pass filtering at 2 kHz was always applied off-line based on FFT before data analysis.

EXPERIMENTAL RESULTS AND ANALYSIS

Instantaneous pressure fluctuation signals, as a parameter, reflect the complexity and nonlinearity of turbulent flow characteristics, to which more attention had been paid in chemical engineering (Sun *et al*., 2006; Xu *et al*., 2004). The profiles of the pressure fluctuation time series under different conditions were illustrated as in Figure 3. From the subplots of the time series of pressure signals, the turbulent characteristics in the KSM were fully embodied. As shown in Figure 3a for different Reynolds numbers at z=620 mm and r/R=0.5, the fluctuation amplitudes and average values of the pressure time series obviously increased as the Reynolds number of the inlet flow increased. The effect of radial positions was revealed in Figure 3b. Because of the redistribution of fluid in the radial and tangential directions, a radial secondary flow is generated. The average values of the pressure time series first increased then decreased and lastly increased. The tube wall pressure series which satisfied r/R=1.0 had maximum average value. From Figure 3c, we find that the average gauge pressure of the fluid has a sharp increase at the second middle cross section CS2 because of the helical turbulent structure. But the average decreased as the axial positions increased. At CS6, the fourth middle cross section, the average values were smaller than the ones at CS1, which means that the intensification ability for turbulence had been achieved. At the same time, the averages at the transitions were larger than the ones at middle cross section, which indicated that the transition zones have better mixing performance. This is because the liquid was split at the leading edge and recombined at the trailing edge of the elements (Kumar *et al*., 2008; Mårten *et al*., 2006, 2008).

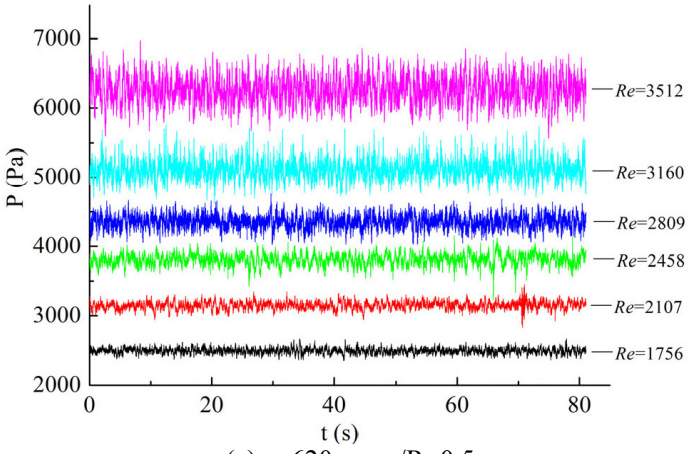

(a) z=620 mm r/R=0.5

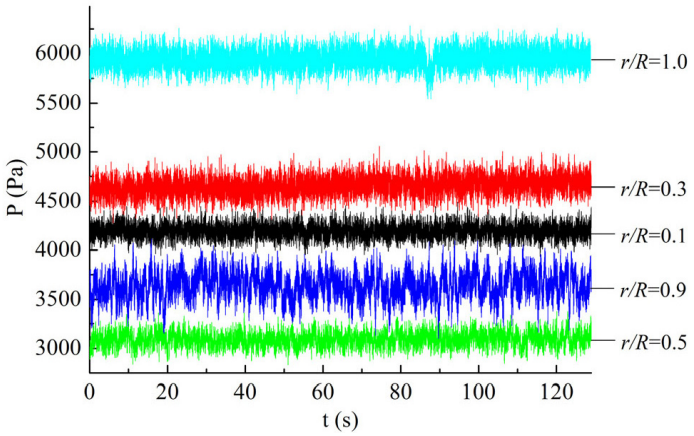

(b) z=100 mm Re=3160

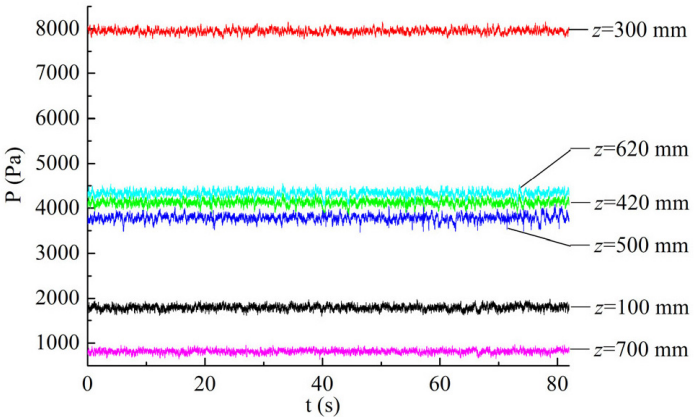

(c) Re=2809 r/R=0.3

Figure 3: The profiles of pressure fluctuation time series under different condition

Hilbert Spectrum Analysis of the Pressure Time Series Under Different Reynolds Numbers

In order to evaluate the effect of inlet flow rates, Empirical Mode Decomposition of the pressure time series at z=500 mm and r/R=0.5 is shown in Figure 4. Empirical mode decompositions are similar to wavelet decomposition. From Figure 4, the pressure fluctuation signals are decomposed into multi-scale signals. The number of IMFs ranged from 9 to 11 with the trend term omitted.

This phenomenon can be explained in terms of the following two aspects. On the one hand, the decomposition process will lead to the inconsistency of the number of iterations by the stopping criterion of sifting for EMD. On the other hand, the pressure signal contains different fluctuation components which will produce varying numbers of IMFs. As can be seen from Figure 4(a)~4(c), the IMFs from top to bottom show that the pressure fluctuations are from short periods to long periods, high frequency to low frequency, which give an expression of the filtering properties of the EMD method. Besides, the larger fluctuation amplitudes in a Kenics Static Mixer generally occur in C_4 to C_8 with the increase of inlet flow rates, which means these IMFs components control and determine the fluid motion properties. For the quantitative analysis of the energy of each IMF, the Mean Square Energy (MSE), as an estimation measure, was defined as follows:

$$MSE_j = \sum_{t=0}^{T} C_j(t) \Big/ N \tag{13}$$

where N, T and j represent the length of the pressure series, the sampling time and the order of the IMF, respectively.

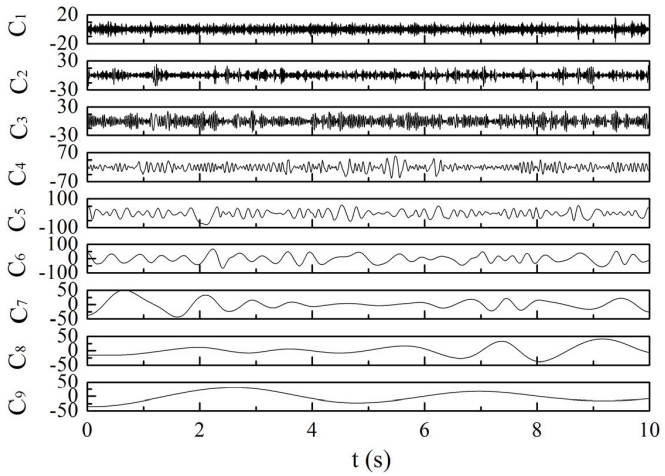

(a) z=500 mm, r/R=0.5 and Re=2107

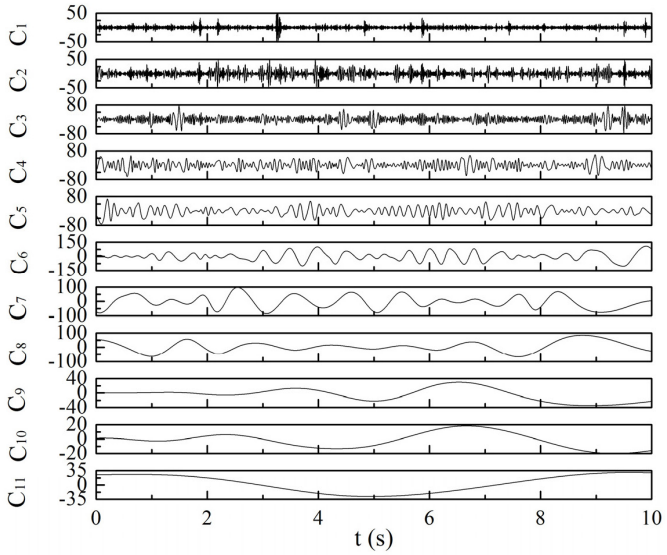

(b) z=500 mm, r/R=0.5 and Re=2458

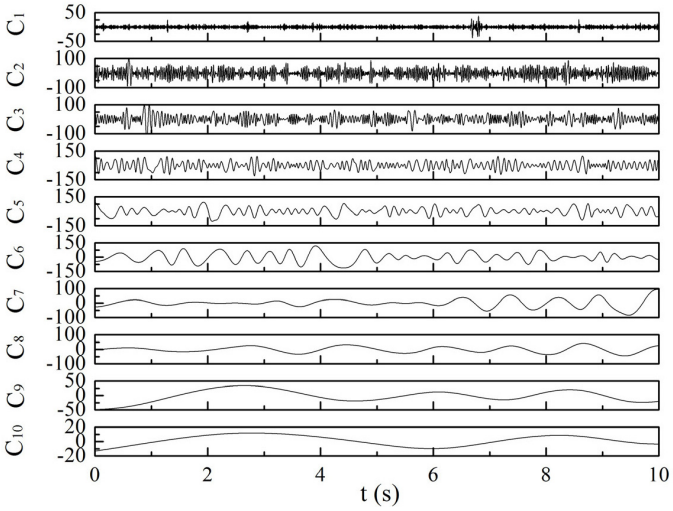

(c) z=500 mm, r/R=0.5 and Re=2809

Figure 4: Empirical Mode Decomposition of pressure time series at z=500 mm, r/R=0.5

Considering the smaller energy ratio which the C_{10} and the higher order IMFs have, the energy distributions of components C_1 ~ C_9 are shown in Figure 5 and 6 in order to compare the energy value and the energy ratio on the same scale under different Reynolds numbers. The frequency bands for components C_1 ~ C_9, corresponding to IMF1 ~ IMF9, are listed in Table 1.

As illustrated in Figure 5, the energy values of each scale IMF have an increasing tendency which indicates that the fluid turbulence and mixing were enhanced as the inlet Reynolds number increased. Comparisons of the energy distribution under different Reynolds numbers indicate that the component of C_6 has maximum energy, which indicates that IMF6 contains the most important fluid dynamics information. Nevertheless, IMF1 and IMF9 always have similar energy values, the most probable interpretation being that IMF1 and IMF9 are two characteristic components of the pressure signal and also reflect two kinds of inherent characteristics of fluid motion in KSM.

Figure 6 shows that the energy ratios profiles of each IMF component under different flow rates. With the variation of Reynolds number, the energy ratios of IMF1 are always the smallest one which indicates that the highest frequency fluctuations in KSM play a less role in fluid turbulence. In addition, the energy ratios of IMF6 maintain the relatively stable values and the change from minimum to maximum is only 2% in total (26% to 28%), which emphasizes the fact that the 6th scale signals represent the forced scale vortex movement in KSM under different Reynolds numbers.

The pressure time series under different Reynolds numbers are processed by Hilbert Transform, and the Hilbert Spectra and Marginal Spectra are showed in Figure 7. In Figure 7, the left graphs are Hilbert Spectra and the corresponding Marginal Spectra are placed on the right side. As can be seen from the Marginal Spectra, most energy of pressure signals is concentrated in less than 40 Hz, which indicates that the pressure fluctuations in KSM are mainly in low frequency. In Hilbert Spectra, the distributions of time-frequency-amplitude within 50 Hz are showed for observation clear. In the Hilbert Spectrums, the horizontal axis is instantaneous time, the vertical axis is instantaneous frequency, and the gray scale of each point in the image qualitatively describes the amplitude of instantaneous pressure fluctuations. The larger the amplitude is, the darker the color is. The signals without 10 Hz distributed randomly and the amplitudes of pressure fluctuations are smaller, while they show a reserve result for the signals within 10 Hz. This is because that eddy motions with low frequency and high power were produced by couple effect between helical blades and tube wall. At the meantime, a mass of small scale vortexes and irrotational fluid micelles which have high frequency and low energy are superimposed on the macro scale eddy. In Marginal Spectra, the energy of the pressure signals in KSM didn't decrease gradually when the frequency band increased higher. In addition to the low frequency fluctuation caused by large scale vortex, the increment of energy also occurs in the frequency region about 30 Hz.

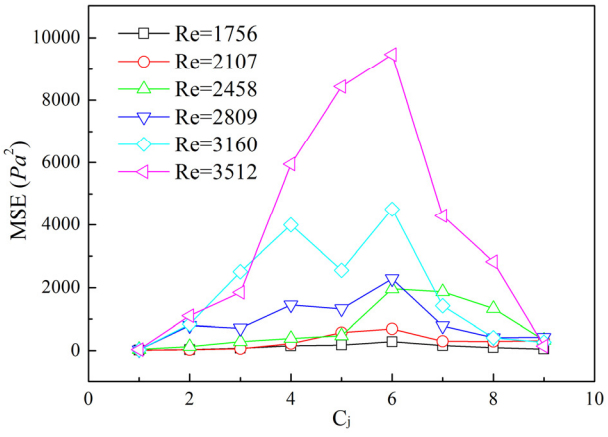

Figure 5: The MSE distribution for different IMFs

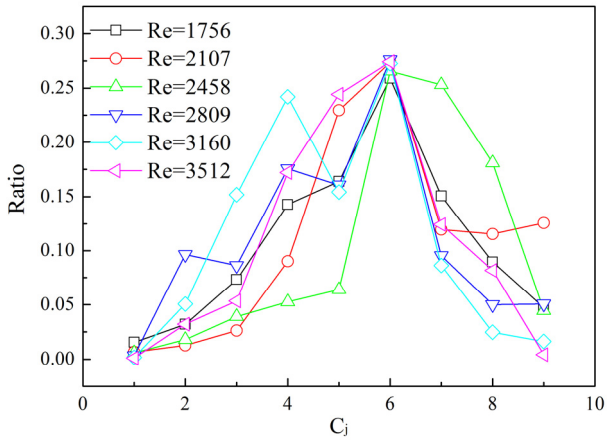

Figure 6: The energy ratio for different IMFs

Table 1: The different intrinsic mode functions and their relevant frequency band

Parameters	IMF1	IMF2	IMF3	IMF4	IMF5	IMF6	IMF7	IMF8	IMF9
Frequency band (Hz)	125-250	62.5-125	31.25-62.5	15.63-31.25	15.63-31.25	7.82-15.63	3.91-7.82	1.96-3.91	0.98-1.96

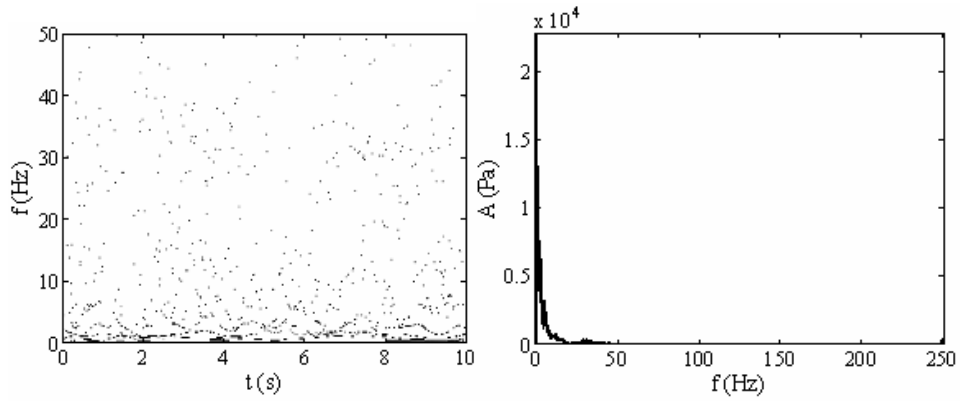

(a) z=500 mm, r/R=0.5 and Re=2107

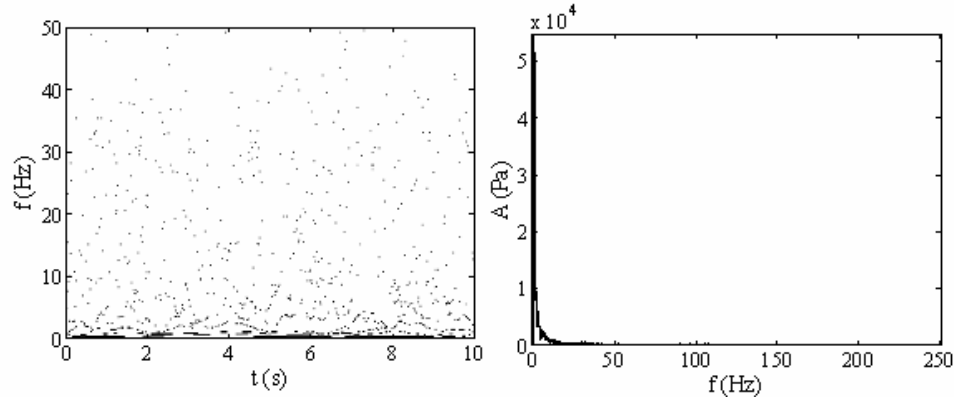

(b) z=500 mm, r/R=0.5 and Re=2458

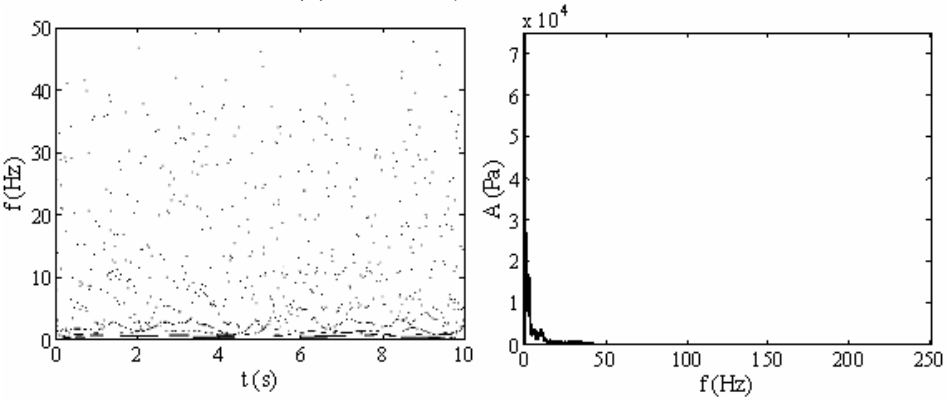

(c) z=500 mm, r/R=0.5 and Re=2809

Figure 7: The Hilbert Spectrum and Marginal Spectrum under different Reynolds numbers

Figure 8 shows the partial enlarged detail of the Marginal Spectrum for Figure 7(a). In Figure 8, the frequency region of 30~35 Hz has a relatively high energy distribution. Although the energy value is not very high, it illustrates the existence of other scales of fluid motion with obvious frequency characters except the largest scale vortex motion. In order to quantitatively describe the energy distributions for the given frequency band, the frequency in the Marginal Spectrum is divided into 6 parts and the result is shown in Table 2.

In Table 2, the energy ratio of fluid movements in 0~10 Hz reaches the maximum for the different Reynolds numbers, which represent the existence of large scale vortex motion in helical pipes. As far as the different scales are concerned, the eddies that consisted of 10~20 Hz and 20~40 Hz fluctuation signals were considered to be the meso-scale and small-scale eddies, respectively, while the frequency of micro scale micelles with random fluctuations was concentrated above 40 Hz.

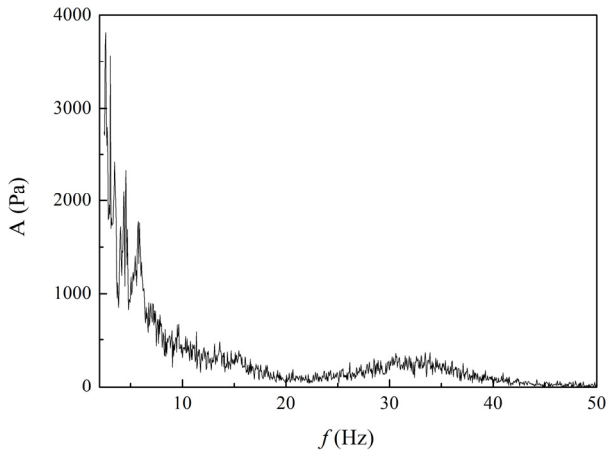

Figure 8: The partial enlarged detail of the Marginal Spectrum for Figure 7(a)

Table 2: The energy ratio of each frequency band under different Reynolds numbers

Re	Energy Ratio %					
	0~10 Hz	10~20 Hz	20~30 Hz	30~40 Hz	40~50 Hz	50~250 Hz
1756	73.47	8.10	4.34	6.23	1.23	6.63
2107	79.73	6.95	2.79	3.57	1.10	5.86
2458	82.34	6.13	3.19	2.98	0.94	4.42
2829	71.43	12.4	6.50	5.98	1.13	2.56
3160	74.00	11.80	5.44	5.10	1.12	2.54
3512	78.32	10.38	4.33	4.36	0.83	1.77

When the Reynolds number varies from 1759~2458 and 2809~3512, the energy ratios within 10 Hz increase while the values within other frequency bands decrease. This can be explained because the increment of the flow rate results in the increment of the energy of large scale eddies, which indicates that the vortex motions are gradually strengthened and the flow state evolves toward a steady state. When the flow rate changes from 2458~2809, the energy ratio within 10 Hz decreases which is contrary to 10-40 Hz. This process indicates that diffusion between large scale eddies occurs and cascade processes of different scale eddies were intensified.

Hilbert Spectrum Analysis of Pressure Time Series Under Different Radial Positions

In order to compare the level of pulsation, instantaneous pressure fluctuations based on removal of mean values can be obtained by constructing all IMFs without residual $r_n(t)$. In this paper, the intensity of instantaneous pressure fluctuation E based on removal of means is defined as follows:

$$E = \sum_{t=0}^{T} \left| s(t) - r_n(t) \right| \tag{14}$$

Figure 9 shows that the intensity distribution at different radial positions in the semi-circular cross section CS4 (z=500 mm) and Re=2809. In the Figure, there are two obvious peaks at r/R=0.2 and 0.8. Because of the effect of free vortex at r/R=0.1 (Kumar *et al*., 2008), fluid eddies move on an adverse pressure gradient in the radial direction. As a result, the energy consumption for viscous resistance is greater. Due to the effect of macro scale eddy viscosity induced by shear stress, the intensity of pulsation increases at r/R=0.2. Therefore, the intensity value E reaches the local minimum at r/R=0.3, except both endpoints. This means that the vortex core of the largest vortex may appear at or near r/R=0.3. With the radial distance increasing, the measured points moved away from the vortex core, and the intensity level of the fluctuation became bigger and bigger. The effect of forced vortex was not replaced by the effect of free vortex until r/R=0.8. A mass of random fluctuations of meso- and small-scale vortexes get energy from the large scale vortex and the pulsation energy reaches a maximum. When the value of r/R was above 0.8, the fluctuation intensity E decreased. The measured point came into the boundary layer when the value of r/R reached 1.0, and the level of pulsation reaches a minimum.

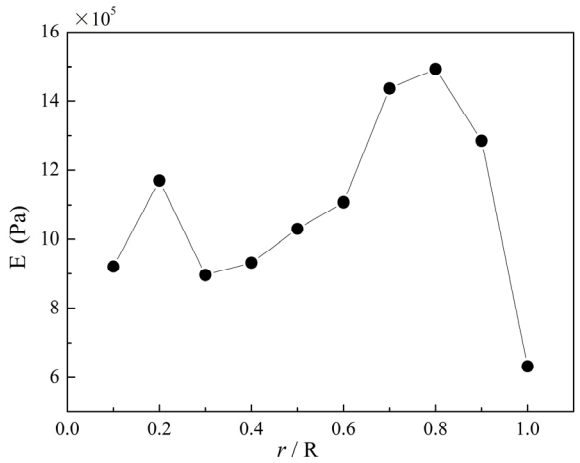

Figure 9: Intensity of instantaneous pressure fluctuation E in different radial positions

The Hilbert-Huang transforms of pressure signals at r/R=0.3, 0.8, 1.0 are shown in Figure 10, respectively. As can be seen from the left Hilbert Spectra and Marginal Spectra on the right side, the frequency distribution is still concentrated in less than 40 Hz. The above mentioned method is still used to quantitatively describe the energy ratio of each frequency band, and the result is shown in Table 3. For the pressure fluctuation signal which has a range of 0~10 Hz, the energy ratio reaches the maximum at r/R=0.3, which indicates again that the fluid motion is relatively stable and the vortex core of the forced vortex appeared near at this point. The analysis result tallies with Figure 9. As the radial measured point varied from 0.3R to 0.6R, the energy ratio within 10 Hz gradually decreases, contrary to the frequency bands of 10~40 Hz. Because of the effect of centrifugal force of the forced vortex, the tangential velocity and viscous shear stress increase as the measured points moved away from the vortex core. Small vortexes were formed and coupled with the main vortex, resulting in the increment of the overall pulsation energy and decrement of the low frequency energy ratio. From 0.6R to 0.8R, the energy ratios of 0~10 Hz and 30~40 Hz increase, while the ones of 10~30 Hz decrease. This is because the scales of vortices superimposed on the macro vortex (forced eddies) gradually become smaller from 0.6R to 0.8R, and the random vibrations with low amplitude become more and more prevalent. In the boundary layer, the pressure fluctuations at r/R=1.0 are mainly caused by the combined action of the low frequency and large-scale coherent structures and the random motion of micro-scale vortexes. Therefore, the energy ratios of 0~10 Hz and above 40 Hz became higher.

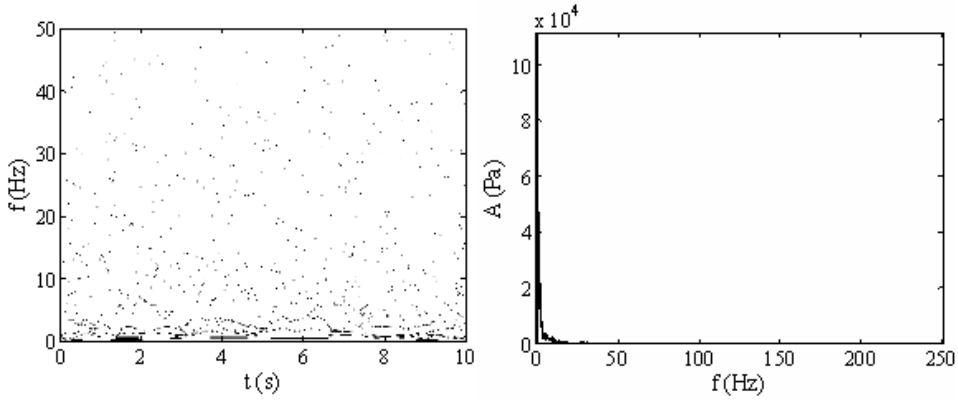

(a) z=500 mm, Re=2809 and r/R=0.3

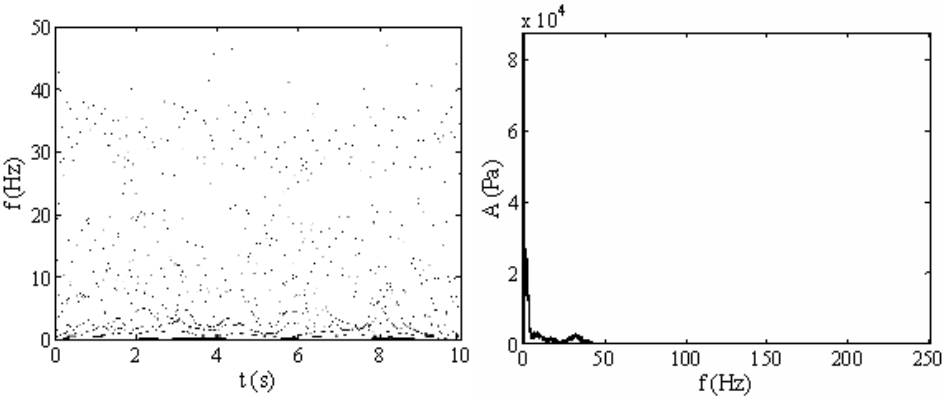

(b) z=500 mm, Re=2809 and r/R=0.8

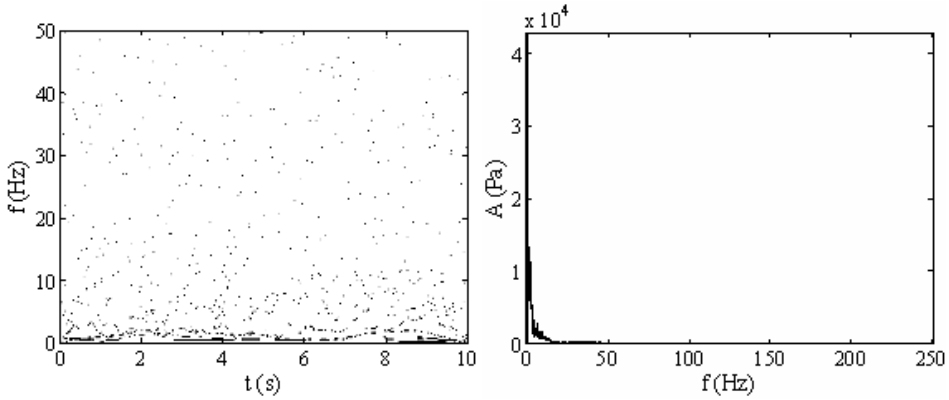

(c) z=500 mm, Re=2809 and r/R=1.0

Figure 10: The Hilbert Spectrum and Marginal Spectrum at different radial positions

Table 3: The energy ratio of each frequency band at different radial positions

r/R	Energy Ratio %					
	0~10 Hz	**10~20 Hz**	**20~30 Hz**	**30~40 Hz**	**40~50 Hz**	**50~250 Hz**
0.1	73.37	9.97	5.99	6.25	1.34	3.08
0.2	77.20	11.39	4.31	3.26	0.80	3.04
0.3	80.15	8.54	3.26	2.73	1.05	4.26
0.4	75.33	9.32	5.80	5.45	1.05	3.05
0.5	71.43	12.04	6.50	5.98	1.13	2.56
0.6	68.77	13.12	7.89	6.61	1.14	2.39
0.7	69.28	13.15	7.55	7.44	0.76	1.82
0.8	70.16	10.19	7.26	10.66	0.63	1.10
0.9	75.45	12.01	6.09	3.08	0.82	2.54
1.0	78.94	7.25	3.08	3.06	1.85	5.20

Hilbert Spectrum Analysis of Pressure Time Series Under Different Axial Positions

The distribution of pressure fluctuations in different axial positions under Re=3512 and r/R=0.5 was analyzed. Figure 11 shows the distribution of instantaneous pressure fluctuation intensity E with the mean value of the pressure series removed. CS1, CS2, CS4 and CS6 are the middle cross sections of the 1st to the 4th mixing element, respectively, while CS3 and CS5 are 20 mm away from the inlet cross section of the 3rd and the 4th mixing element, respectively. In Figure 11, the intensity of instantaneous pressure fluctuation E increases due to the reinforcing action of mixing elements when the liquid passed CS2. In addition, the energy values E of CS3 and CS5 are much larger than the ones of CS4 and CS6. That is because, when the liquid enters the adjacent mixing element, the rotation direction of the vortexes is changed and the fluid is split again by the mixing element edges, which causes a mass of pressure fluctuations. The intensity of instantaneous pressure fluctuation E of CS6 is smaller than that of CS4, which indicates that the pressure drop increases with the increase of the number of mixing elements.

From the Hilbert Spectra and Marginal Spectra of the pressure fluctuation signals mentioned above, the energy distribution above 90% is still concentrated in less than 40 Hz with the variation of axial position. The energy ratios of each frequency band are shown in Table 4.

In Table 4, the energy ratio within 10 Hz increases from CS1 to CS2, which indicates that there is a more stable eddy motion at CS2. At CS3 and CS5, the energy ratios within 10 Hz decrease, which is contrary to the other frequency bands. This is mainly because the fluid streams were affected by the entrance effect (cutting and direction changing). At CS4 and CS6, the energy ratios of 0~10 Hz increase, which means that, after the entrance to the mixing element, the fluid movement recombined and reached a relatively stable state again. Observing the group data of CS3-CS4 and CS5-CS6, it is not difficult to see that the energy ratios of each frequency band are similar in each group. The results indicate that the fluid movements in these two periodic mixing-elements are similar. Therefore, the fluid motion can reach a relatively stable state on the macro-level after 3~4 mixing elements in the KSM.

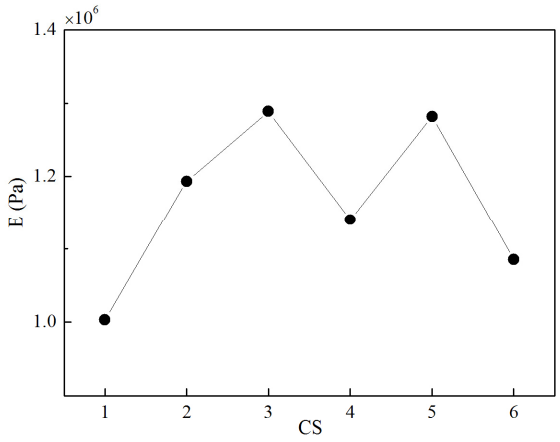

Figure 11: Intensity of instantaneous pressure fluctuation E in different axial positions

Table 4: The energy ratio of each frequency band at different axial positions

CS	Energy Ratio %					
	0~10 Hz	10~20 Hz	20~30 Hz	30~40 Hz	40~50 Hz	50~250 Hz
1	70.12	14.42	5.69	6.61	1.09	2.07
2	75.97	13.36	3.34	2.69	1.17	3.47
3	73.44	11.34	5.49	5.38	1.25	3.11
4	79.15	9.82	4.54	3.96	0.85	1.68
5	73.64	11.41	5.85	5.14	1.24	2.72
6	78.57	9.84	4.94	3.28	0.78	2.59

CONCLUSIONS

In order to understand the intrinsic features of the non-linear behavior of a fluid system, the Hilbert-Huang Transform based on Empirical Mode Decomposition was first introduced to describe the time-frequency features of the pressure fluctuation in the KSM. The Hilbert spectra of the pressure fluctuation time series were quantitatively evaluated under different Reynolds numbers and radial and axial positions, respectively. The experimental results show that the frequency distributions of the pressure fluctuation signals in KSM were mainly concentrated in less than 40 Hz, while more than 68% of the energy of the fluctuation signals was mainly concentrated within 10 Hz. Compared with other IMFs under different flow rates, IMF6, with a range of 7.82~15.63 Hz representing the forced scale vortex movement, has the maximum MSE and a relatively stable energy ratio. As the inlet Reynolds number increases, the low frequency (0~10 Hz) energy ratio increases except for the state of Re=2458~2809 because of the obvious energy diffusion.

From the Hilbert spectrum profiles of the pressure time series, the pressure intensity reached the local minimum and the low frequency component with a range of 0~10 Hz had the maximum energy ratio at r/R=0.3. As a result, the vortex core of the macro scale vortex appeared at nearly r/R=0.3 and the effect of free vortexes appeared at r/R>0.8. Based on removal of the mean values of time series, the largest pulsation amplitudes are at r/R=0.8, which indicated that the smaller scale free vortexes had much higher frequency fluctuations. In addition, as the radial dimensional distance increases away from the vortex core, the energy ratios of 10~40 Hz increase except for r/R=1.0, which indicates that the smaller scale fluid micelles become more and more important.

From the comparisons of the pressure signals at different axial positions, the intensifying ability for turbulence was immediately revealed. The fluctuation energy of pressure at the leading edges was larger than at other axial positions because of the recombined streams. The pressure fluctuation signals at CS3 and CS5 or CS4 and CS6 have similar frequency distributions and energy proportions in each frequency band. Considering the periodical arrangement of the mixing elements, the fluid motion can reach a relatively stable state on the macro-level after 3~4 mixing elements in the KSM.

ACKNOWLEDGMENT

This project is supported by National Natural Science Foundation of China (No.21106086), the Special Program for local universities development of central finance of China (No.2050205), the Natural Science Foundation of Liaoning Province (No.201102175), the Higher Education Program Funds for the Key Laboratory Research of Liaoning Province (No. LS2010124).

NOMENCLATURE

$a_j(t)$	amplitude function	Pa
$C_j(t)$	Intrinsic Mode Functions	Pa
ES	marginal energy spectrum	Pa^2
$h(\omega)$	marginal spectrum	Pa
L	the length of the mixing-element	mm
MSE	Mean Square Energy	Pa^2
N	the number of mixing elements	
N	length of time series	
P	pressure	Pa
$p_m(t)$	average of upper and lower envelopes	Pa
Q	flow rate	$L \cdot h^{-1}$
R	the radial distance of measured point	mm
$rr_n(t)$	residual function	Pa
R	radius of the mixing element	mm
Re	Reynolds number	
S	pressure series	Pa
T	time	s
T	sampling time	s
x, y, z	cartesian coordinates	mm
X, Y	cartesian coordinates	mm

Greek Symbols

A	angle between axial cross-section and the positive axis	
ω	instantaneous frequency	

REFERENCES

Byrde, O., Sawley, M. L, Optimization of a Kenics static mixer for non-creeping flow conditions. Chem. Eng. J., 72, 136-169 (1999).

Chen, S. J., In-line, continueous mixing and processing of cosmetic products. J. Cosmet. Soc., 24, 639-653 (1973).

Chen, Z. P., Zhang, Y. X., Lin, X. H., Handbook for design and selection of stirred and mixing equipments. Chem. Ind. Press (Beijing), 434-440 (2004).

Costa, M., Goldberger, A. L., Peng, C. K., Multiscale entropy analysis of complex physiologic time series. Phys. Rev. Lett., 89, 68-102 (2002).

Douroumis, D., Fahr, A., Enhanced dissolution of Oxcarbazepine microcrystals using a static mixer process. Colloids Surf., B, 59, 208-214 (2007).

Flandrin, P., Rilling, G., Gonçcalvés, P., Empirical Mode Decomposition as a Filter Bank. IEEE Signal Process. Lett., 11, 112-114 (2004).

Gong, B., Bao, Z. P., Zhang, C. M., Wu, J. H., Effect of Number of Mixing Elements on Flow Field in Kenics Static Mixer. CIESC J., 60, 1974-1980 (2009). (In Chinese).

Grace, C. D., Static mixing and heat transfer. Chem. Eng. Process., 52, 57-59 (1971).

Heyouni, A., M., Roustan, Do, Q. Z., Hydrodynamics and mass transfer in gas-liquid flow through static mixers. Chem. Eng. Sci., 57, 3325-3333 (2002).

Hobbs, D. M., Muzzio, F. J., The Kenics static mixer: a three-dimensional chaotic flow. Chem. Eng. J., 67, 153-166 (1997).

Hobbs, D. M., Muzzio, F. J., Reynolds number effects on laminar mixing in the Kenics static mixer. Chem. Eng. J., 70, 93-104 (1998a).

Hobbs, D. M., Muzzio, F. J., Optimization of a static mixer using dynamical system techniques. Chem. Eng. Sci., 53, 3199-3213 (1998b).

Hobbs, D. M., Swanson, P. D., Muzzio, F. J., Numerical characterization of low Reynolds number flow in the Kenics static mixer. Chem. Eng. Sci., 53, 1565-1584 (1998).

Huang, N. E., Shen, Z., Long, S., Wu, M. C., Shih, H. H., Zheng, Q., Yen, N. C., Tung, C. C., Liu, H. H., The empirical mode decomposition and the Hilbert spectrum for nonlinear and non-stationary time series analysis. Proc. R. Soc. Lond. A, 454, 903-995 (1998).

Joshi, P., Nigam, K. D. P., Nauman, E. B., The Kenics static mixer - new data and proposed correlations. Chem. Eng. J. and Biochem. Eng. J., 59, 265-271 (1995).

Jones, S. C., Sotiropoulos F., Amirtharajah A., Numerical modeling of helical static mixers for water treatment. J. Environ. Eng., 128, 431-440 (2002).

Krstic, Darko, M., Wilhelm, H., Koris, A. K., Energy-saving potential of cross-flow ultrafiltration with inserted static mixer: Application to an oil-

in-water emulsion. Sep. Purif. Technol., 57, 134-213 (2007).

Kumar, V., Shirke, V. K., Nigam, D. P., Performance of Kenics static mixer over a wide range of Reynolds number. Chem. Eng. J., 139, 284-295 (2008).

Lehwald, A., Thévenin, D., Zähringer, K., Quantifying macro-mixing and micro-mixing in a static mixer using two-tracer laser-induced fluorescence. Expe. Fluids, 48, 823-836 (2010).

Lisboa, P. F., Fernandes, J., Simões, P. C., Mota, J. P. B., Saatdjian E., Computational-fluid-dynamics study of a Kenics static mixer as a heat exchanger for supercritical carbon dioxide. J. Supercritical Fluids, 55, 107-115 (2010).

Madhuranthakam, C. M. R., Pan, Q. M., Rempel, G. L., Residence time distribution and liquid holdup in Kenics KMX static mixer with hydrogenated nitrile butadiene rubber solution and hydrogen gas system. Chem. Eng. Sci., 64, 3320-3328 (2009).

Mårten, R., Karin, Ö., Christian, T., Effects of geometry and flow rate on secondary flow and the mixing process in static mixers–A numerical study. Chem. Eng. Sci., 61, 6133-6141 (2006).

Mårten, R., Karin, Ö., Christian, T., Influence of viscosity ratio on the mixing process in a static mixer: numerical study. Ind. Eng. Chem. Res., 47, 3030-3036 (2008).

Meng, H. B., Yu, Y. F., Liu, Z. Q., Wu, J. H., Correlation integral of turbulent instantaneous velocity time series in a Kenics static mixer. J. Beijing Univ. Chem. Tech. Nat. Sci. Ed., 36, 97-102 (2009a). (In Chinese).

Meng, H. B., Wu, J. H., Yu, Y. F., Chen, X., Chaotic characteristics of velocity in cutting region of Kenics static mixer. Chemical Engineering, 37, 24-27 (2009b). (In Chinese).

Pahl, M. H., Muschelknautz, E., Static mixer and their applications. Int. Che. Eng., 22, 197-205 (1982).

Pincus, S. M., Approximate entropy as a measure of system complexity. Proc. Natl. Acad. Sci. U. S. A., 88, 2297-2301 (1991).

Pincus, S. M., Approximate entropy (ApEn) as a complexity measure. Chaos, 5, 110-117 (1995).

Pincus, S. M., Goldberger, A. L., Physiological time series analysis: what does regularity quantify? Am. J. Physiol. Heart Circ. Physiol., 266, H1643-H1655 (1994).

Rauline, D., Tanguy, P. A., LeBlévec, J. M., Bousquet, J., Numerical investigation of the performance of several static mixers. Can. J. Chem. Eng., 76, 527-535 (1998).

Richman, J. S., Moorman, J. R., Physiological time-series analysis using approximate entropy and sample entropy. Am. J. Physiol. Heart Circ. Physiol., 278, 2039-2049 (2000).

Saha, S. K., Dutta, A., Friction and heat transfercharacteristics of laminar swirl flow through a circular tube fitted with regularly spaced twisted-tape elements. Int. J. Heat Mass Transfer, 44, 4211-4223 (2001).

Song, H. S., Sang, P. H., A general correlation for pressure drop in a Kenics static mixer. Chem. Eng. Sci., 60, 5696-5704 (2005).

Sun, H. Y., Wu, Y., Xu, C. H., Pressure fluctuation in the submerged circulative impinging stream reactor. Chinese J. Chem. Eng., 14, 428-434 (2006).

Thakur, R. K., Vial, Ch., Nigam, K. D. P., Nauman, E. B., Djelveh G., Static mixers in the process industries-a review. Chem. Eng. Res. and Des., 81, 787-826 (2003).

Visser, J. E., Rozendal, P. F., Hoogstraten, H. W., Beenackers, A. A. C. M., Three-dimensional numerical simulation of flow and heat transfer in the Sulzer SMX staticmixer. Chem. Eng. Sci., 54, 2491-2500 (1999).

Yu, Y. F., Meng, H. B., Wu, J. H., Delay time correlation of velocity fluctuation signal in the Kenics static mixer. J. Petrochem. Univ., 21, 73-77 (2008). (In Chinese).

Wilkinson, W. L., Cliff, M. J., An investigation into the performance of a static inline mixer. Proc. 2nd Euro. Conf. Mix., Cambridge, UK, 15-29 (1997).

Wu, J. H., Zhang, C. M., Jin, D., Sun, D.,Gong, Bin., Experimental study on turbulence properties in a Kenics static mixer. Chin. J. Process Eng., 8, 714-718 (2008). (In Chinese).

Wu, J. H., Xu, F., Zhang, C. M., Gong, B., Characteristic of pulse velocity of turbulenec in a SK mixer. Chem. Eng., 37, 30-33 (2009). (In Chinese).

Wu, J. H., Meng, H. B., Yu, Y. F., Gong, B., Fractal identification of instantaneous velocity time series in Kenics static mixer. J. Sichuan Univ. Eng. Sci. Ed., 42, 220-226 (2010). (In Chinese).

Wu, J. H., Meng, H. B., Yu, Y. F., Gong, B., Multi-scale and multi-fractal characteristics of tube-pressure signals in Kenics static mixer. CIESC J., 60, 1965-1973 (2009). (In Chinese).

Wu, Z. H., Huang, N. E., A Study of the Characteristics of white noise using the empirical mode decomposition method. Proc. R. Soc. Lond., A, 460, 1597-1611 (2003).

Xu, J., Bao, X. J., Wei, W. S., Shi, G., Shen, S. K., Bi, H. T., Grace, J. R., Lim, C.J., Statistical and

frequency analysis of pressure fluctuations in spouted beds. Powder Technology, 140, 141-154 (2004).

Zalc, J. M., Szalai, S. E., Muzzio, F. J., Jaffer, S., Characterization of flow and mixing in an SMX static mixer. AIChE. J., 48, 427-436 (2002).

Zhang, C. M., Wu, J. H., Gong, B., Flow resistance researches for SK static mixer tube of turbulent flow. Chem. Eng., 34, 27-30 (2006). (In Chinese).